



HAL
open science

Derivation of Hamaker Dispersion Energy of Amorphous Carbon Surfaces in Contact with Liquids Using Photoelectron Energy-Loss Spectra

Christian Godet, Denis David

► **To cite this version:**

Christian Godet, Denis David. Derivation of Hamaker Dispersion Energy of Amorphous Carbon Surfaces in Contact with Liquids Using Photoelectron Energy-Loss Spectra. *Brazilian Journal of Physics*, 2017, 47 (6), pp.594 - 605. 10.1007/s13538-017-0521-0 . hal-01655081

HAL Id: hal-01655081

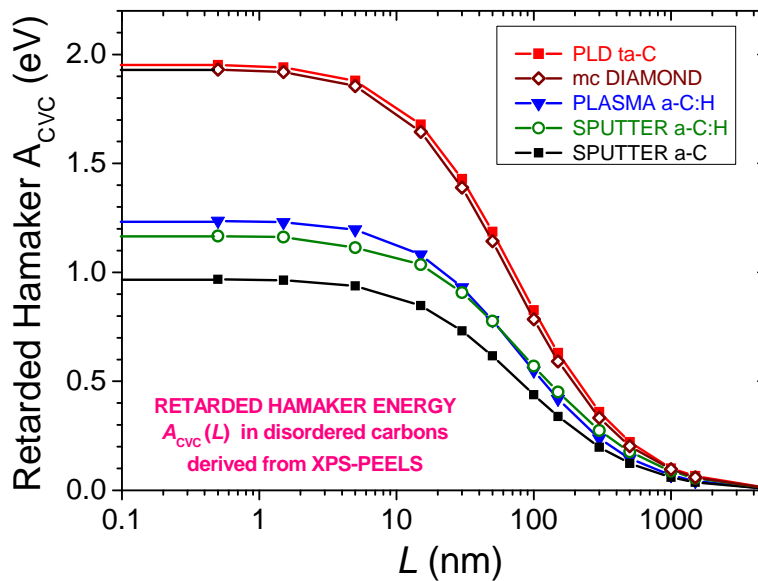
<https://univ-rennes.hal.science/hal-01655081>

Submitted on 5 Dec 2017

HAL is a multi-disciplinary open access archive for the deposit and dissemination of scientific research documents, whether they are published or not. The documents may come from teaching and research institutions in France or abroad, or from public or private research centers.

L'archive ouverte pluridisciplinaire **HAL**, est destinée au dépôt et à la diffusion de documents scientifiques de niveau recherche, publiés ou non, émanant des établissements d'enseignement et de recherche français ou étrangers, des laboratoires publics ou privés.

Graphical Abstract



Derivation of Hamaker dispersion energy of amorphous carbon surfaces in contact with liquids using photoelectron energy-loss spectra

Christian Godet^a, Denis David^b

^a Institut de Physique de Rennes (CNRS UMR 6251), Université Rennes 1, Campus Beaulieu - Bât. 11E - 35042 Rennes (France)

^b Instituto de Física, Universidade Federal da Bahia, Campus Universitário de Ondina, 40.210-340 Salvador, Bahia (Brazil)

Corresponding author : christian.godet@univ-rennes1.fr

Keywords:

Hamaker energy,
 amorphous carbon,
 XPS,
 energy loss spectroscopy,
 dielectric function

PACS : 79.60.HT, 68.35.Md, 82.80.Pv, 61.85.+p

ABSTRACT

Hamaker interaction energies and cutoff distances have been calculated for disordered carbon films, in contact with purely dispersive (diiodomethane) or polar (water) liquids, using their experimental dielectric functions $\varepsilon(q, \omega)$ obtained over a broad energy range. In contrast with previous works, a q -averaged $\langle \varepsilon(q, \omega) \rangle_q$ is derived from photoelectron energy loss spectroscopy (XPS-PEELS) where the energy loss function (ELF) $\langle \text{Im}[-1/\varepsilon(q, \omega)] \rangle_q$ is a weighted average over allowed transferred wave vector values, q , given by the physics of bulk plasmon excitation. For microcrystalline diamond and amorphous carbon films with wide range of ($\text{sp}^3 / \text{sp}^2+\text{sp}^3$) hybridization, non-retarded Hamaker energies, A_{132} ($L < 1$ nm), were calculated in several configurations, and distance and wavenumber cutoff values were then calculated based on A_{132} and the dispersive work of adhesion obtained from contact angles. A geometric average approximation, $H_{0\text{ CVL}} = (H_{0\text{ CVC}} H_{0\text{ LVL}})^{1/2}$, holds for the cutoff separation distances obtained for Carbon-Vacuum-Liquid (CVL), Carbon-Vacuum-Carbon (CVC) and Liquid-Vacuum-Liquid (LVL) equilibrium configurations. The linear dependence found for A_{CVL} , A_{CLC} , A_{CLV} values as a function of A_{CVC} , for each liquid, allows predictive relationships for Hamaker energies (in any configuration) using experimental determination of the dispersive component of the surface tension, γ_{CV}^d , and a guess value of the cutoff distance $H_{0\text{ CVC}}$ of the solid.

1. Introduction

Lifshitz theoretical formalism [1, 2] to calculate dispersion forces between electrically neutral macroscopic bodies based on their dielectric functions, $\varepsilon(q, \omega)$, has been considerably developed over the last sixty years to understand experiments in condensed matter physics, colloid science, self-assembly, biology and surface physics [3-5]. Particular interest has been devoted to some applications of carbon-based materials including stability of carbon black or nanocarbon dispersions [6-8], nanocomposite strength [9] and tribology of magnetic disk coatings [10-12].

The Lifshitz equation for van der Waals (vdW) interaction energy per unit area as a function of separation distance, L , between parallel planar half-spaces 1 and 2 separated by intervening medium 3, is given by:

$$E_{132} = -A_{132}(L) / 12\pi L^2 \quad (1)$$

where $A_{132}(L)$ is the Hamaker energy. Simple geometrical corrections have been established for different configurations [3].

Dispersion forces are related to changes of the zero-point energy of the electromagnetic field due to spontaneous electromagnetic fluctuations and their correlations [3, 13]; in condensed matter, they can alternatively be represented in terms of surface modes excited in macroscopic homogeneous dielectric bodies [3, 14]. The free energy of the system being described as a sum over all electromagnetic modes, Laplace equation in charge-free homogeneous space can be solved with boundary conditions including continuity of potential Φ and normal component of electrical displacement $\varepsilon (\nabla \Phi)_\perp$ [3, 14, 15]. In this context, the Hamaker energy, $A_{132}(L)$, is defined by [1-3, 16]

$$A_{132}(L) = -\frac{3}{2} k_B T \sum_{n=0}^{\infty} \int_{r_n}^{\infty} x \left\{ \text{Ln}[1 - \Delta_{13}^* \Delta_{23}^* e^{-x}] + \text{Ln}[1 - \Delta_{13} \Delta_{23} e^{-x}] \right\} dx \quad (2)$$

where k_B is the Boltzmann constant. The prime symbol indicates that the zero-frequency term of the interaction has to be multiplied by 1/2. The quantities Δ_{jk}^* and Δ_{jk} for the spontaneous electromagnetic fluctuations (Transverse Magnetic and Transverse Electric modes, respectively) at frequency ζ are given by

$$\Delta_{jk}^* = \frac{s_k - s_j}{s_k + s_j} \quad \Delta_{jk} = \frac{\varepsilon_j s_k - \varepsilon_k s_j}{\varepsilon_j s_k + \varepsilon_k s_j} \quad s_k^2 = x^2 + \left(\frac{2L\zeta_n}{c} \right)^2 (\varepsilon_k - \varepsilon_3) \quad (3)$$

where the continuum dielectric response functions, $\varepsilon_K = \varepsilon_K(i\zeta_n)$, are evaluated at imaginary frequencies with $\zeta_n = n 2\pi k_B T / \hbar$ (for $n = 0, 1, 2, \dots$). The expressions given for Δ_{jk}^* and Δ_{jk}

(Eqn. 3) mean that interactions result only from electromagnetic field fluctuations at identical frequencies ζ_n in each material. Here, parameter $r_n = 2L\zeta_n (\epsilon_3)^{1/2} / c$ accounts for retardation effects due to the finite speed of light, c . The London dispersion function, $\varepsilon(i\zeta_n)$, is defined via the Kramers-Krönig (KK) transform:

$$\varepsilon(i\zeta_n) = 1 + \frac{2}{\pi} \int_0^{\infty} \text{Im}[\varepsilon(\omega)] \frac{\omega d\omega}{\omega^2 + \zeta_n^2} \quad (4)$$

of the dielectric function and requires experimental knowledge of $\varepsilon(q, \omega)$ over several tens of eV. While the quality of experimental data and extrapolation schemes in the extreme ultraviolet (EUV) energy range have been widely considered [3], the choice of the q wave vector range has seldom been addressed [15, 17-19].

Equation (2) can also be taken in its non retarded form where the interaction energy $E_{132}(L)$ at small distance is [1, 2]:

$$E_{132}(L) = -\frac{k_B T}{2\pi} \sum_{n=0}^{\infty} \int_0^{k_{C(132)}} dk k \left\{ Ln[1 - \Delta_{13}^* \Delta_{23}^* e^{-2kL}] + Ln[1 - \Delta_{13} \Delta_{23} e^{-2kL}] \right\} \quad (5)$$

k is the transverse wave vector of the fluctuating electromagnetic field. The divergence in van der Waals interaction energy $E_{132}(L \rightarrow 0)$ is alleviated by considering minimum separation distance, $H_{0\ 132}$, at equilibrium or alternatively some maximum cutoff wavenumber, given by $k_{0\ 132} \approx (1/H_{0\ 132})$, which better meets thermodynamic constraints [17-18]. This concept of material-specific cutoff wavenumber value has been revisited recently for decane-water-air interfaces [19].

In this work, Hamaker interaction energies and cutoff distances have been calculated for disordered carbon films in contact with purely dispersive (diiodomethane, DIM) or polar (water, W) liquids, using their experimental dielectric functions $\varepsilon(q, \omega)$ obtained over a broad energy range. In contrast with previous works, a q -averaged $\langle \varepsilon(q, \omega) \rangle_q$ is derived from photoelectron energy loss spectroscopy (PEELS) where the energy loss function (ELF) $\langle \text{Im}[-1/\varepsilon(q, \omega)] \rangle_q$ is a weighted average over allowed transferred wave vector values, q , given by the physics of bulk plasmon excitation (see Section 2.1). XPS-PEELS data for C1s photoelectrons are obtained over 50 eV energy loss range in a classical X-ray photoelectron spectroscopy (XPS) experiment, for several well-characterized amorphous carbon (a-C) and microcrystalline diamond (mc-diamond) films with wide range of (sp^3 / sp^2+sp^3) hybridization, optical gap, atom density and hydrogen content (Table 1).

Table 1: Characteristics of a-C and mc-diamond films derived from XPS and SE: $sp^3 / (sp^3 + sp^2)$ hybridization ratio (± 0.05), atom density $N_{AT} = N_{EFF} / 4$ (**Eqn. 9**), ELF peak energy E_p (± 0.3 eV), cutoff wavenumber q_c for plasmon excitation, real dielectric function $\epsilon_1(E = 0)$ (± 0.03), Tauc energy gap E_T (± 0.2 eV) at the onset of optical absorption. Dispersive surface energy γ_{CV}^d (± 2 mJ/m²) was derived from the measured contact angle θ_{DIM} ($\pm 1^\circ$) [**21**].

<i>Disordered carbon</i>	$sp^3 / (sp^2 + sp^3)$	N_{AT} (10^{22} at.cm ⁻³)	E_p (eV)	q_c (nm ⁻¹)	$\epsilon_1(E = 0)$	E_T (eV)	θ_{DIM}	γ_{CV}^d (mJ/m ²)
a-C Sputtered	0.18	9.9	28.0	14.1	5.29	0.4	31.4°	43.8
a-C:H Plasma	0.88	10.3	24.0	13.4	4.00	2.5	47.3°	35.9
a-C:H Sputtered	0.13	9.3	26.5	13.9	3.60	0.5	29.5°	44.6
ta-C PLD	0.52	14.5	31.0	14.6	6.25	0.6	38.5°	40.5
mc-diamond HF-CVD	1.0	17.6	34.5	15.1	5.66	5.5	30.9°	44.0

The methodology given in **Sections 2.2** and **2.3** allows calculation of non-retarded Hamaker energies in several configurations (including C-Vacuum-C, C-Water-C, C-DIM-C, C-Vacuum-Water, C-Vacuum-DIM) and wavenumber cutoff values were then calculated based on A_{132} and the dispersive work of adhesion obtained from contact angles. For liquid water and diiodomethane, oscillator models of the dielectric function and London dispersion [**19-20**] have been used. This set of results for disordered carbon surfaces provides cutoff separation distance, $H_{0\ 132}$, and wave number, $k_{0\ 132}$, for Carbon-Vacuum-Liquid (CVL), Carbon-Vacuum-Carbon (CVC) and Liquid-Vacuum-Liquid (LVL) configurations (**Section 3**). Some predictive relationships for amorphous carbon films in contact with a liquid are discussed in **Section 4**.

2. Methodology

Experimental details on amorphous carbon and microcrystalline diamond film deposition, spectroscopic ellipsometry (SE) analysis, contact angle (CA) measurements and XPS-PEELS characterizations have been given in previous reports [**21-25**]. Amorphous carbon films are usually classified into different families according to the mean ion energy and hydrogen atom flux during the deposition process [**26, 27**]. In contrast with the sp^2 -rich films grown by sputtering techniques (a-C or a-C:H), the sp^3 -rich carbon material grown by pulsed laser deposition (PLD) is named here as ta-C for "tetrahedrally-bonded amorphous carbon". Plasma decomposition of hydrocarbons

produces sp^3 -rich hydrogenated carbon (plasma a-C:H). Very smooth surfaces are obtained for all the above techniques, with sub-nm roughness as obtained from Atomic Force Microscopy [23, 28]. In contrast, boron doped mc-diamond films ($[B] \approx 10^{19} \text{ cm}^{-3}$) grown by hot filament chemical vapor decomposition (HF-CVD) of hydrocarbons have a rough and strongly faceted topography with pyramidal crystallite height smaller than 0.5 micron [24].

In a previous work, contact angles have been measured with purely dispersive or polar liquids; measurement reproducibility ($\pm 1^\circ$) provides error bars on dispersive surface energy, γ_{CV}^d , smaller than 2 mJ/m^2 [21]. Surface energies were correlated with the $sp^3 / (sp^2 + sp^3)$ average hybridization deduced from X-ray photoelectron spectroscopy, after decomposition of C1s spectra into two Voigt peaks separated by 0.77 eV [21]. XPS survey spectra show some oxygen contamination on sputtered a-C, while other carbon surfaces have very small contamination from the ambient ($[O] < 3 \text{ at.}\%$), well below one monolayer. The atom density, N_{AT} , of amorphous carbon films has been tentatively estimated from the $(\sigma+\pi)$ plasmon peak energy observed in photoelectron energy loss spectra or from sum rules ($N_{AT} = N_{EFF}/4$) (Table 1) [25].

In the following, XPS-PEELS data acquisition and analysis are briefly recalled and the methodology used to relate contact angle measurements with Hamaker energies is detailed. Two methods will be compared in order to retrieve the cutoff separation distance, $H_{0\ 132}$, and cutoff wave number, $k_{0\ 132}$, for Carbon-Vacuum-Liquid (CVL), Carbon-Vacuum-Carbon (CVC) and Liquid-Vacuum-Liquid (LVL) configurations.

2.1 PEELS method and q -averaged dielectric function

Photoelectron Energy Loss Spectroscopy (XPS-PEELS) is a highly valuable non-destructive tool which extends the analytical capabilities of XPS (chemical composition obtained from core level peak intensities) to provide detailed insight in electronic properties (near-surface dielectric function derived from kinetic energy losses of photoelectrons). Experiments can be performed with usual XPS laboratory spectrometers and do not need monochromatic X-ray source, although the latter is strong advantage in order to obtain accurate (sp^3 / sp^2+sp^3) hybridization ratio of carbon-based materials [21].

In disordered carbons (e.g. amorphous carbon and microcrystalline diamond), the main energy-loss channel is related to excitation of $\sigma+\pi$ plasmon excitations, i.e. the collective oscillation of all valence electrons in the vicinity of their C nucleus [22-25]. XPS-PEELS data are representative of the near-surface material within a few inelastic mean free paths (IMFP); as the C atom density

decreases, the IMFP λ_P (970 eV) increases from 1.2 nm to 1.6 nm, assuming a cutoff plasmon wavenumber, q_C , given by a free electron model [25].

PEELS data analysis is based on self-consistent separation of bulk (BP) vs surface (SP) plasmon excitations, deconvolution of multiple BP losses and evaluation of Bethe-Born sensitivity factors for bulk and surface loss distributions. An inversion algorithm provides several material parameters: (1) energy loss function for BP excitation, (2) dielectric function $\varepsilon(q, \omega)$ of the near-surface material, (3) inelastic mean free path, $\lambda_P(E_0)$, for plasmon excitation, (4) effective number N_{EFF} of valence electrons participating in the plasma oscillation.

Owing to the collective nature of plasmon excitation, the ELF is best described in terms of complex dielectric function, $\varepsilon(\hbar\omega)$, of the solid [29-31]. For electrons travelling through an infinite medium, the differential inverse inelastic mean free path (DIIMFP) is the probability density per unit path length, $K(E_0, \hbar\omega)$, of losing an energy $\hbar\omega$:

$$K(E_0, \hbar\omega) = \frac{1}{\pi a_0 E_0} \int_{q^-}^{q^+} \frac{dq}{q} \text{Im} \left[\frac{-1}{\varepsilon(\omega)} \right] \quad (6)$$

where E_0 is the initial kinetic energy of the photoelectron, a_0 is the Bohr radius, and q is the wave vector transferred from the electron:

$$q_{\pm} = \left[\frac{2m_0}{\hbar^2} \right]^{1/2} \left[E_0^{1/2} \pm (E_0 - \hbar\omega)^{1/2} \right] \quad (7)$$

are q vector limits imposed by energy and momentum conservation during inelastic scattering. In addition, a cutoff wave vector transfer, q_C , is introduced to account for plasmon decay to single particle excitations ($q_C \ll q_+$) [32].

It is emphasized that the ELF distribution obtained in PEELS analysis is normalized using the KK relationship near $T \rightarrow 0$:

$$\text{Re} \left(\frac{1}{\varepsilon(T)} \right) = 1 - \frac{2}{\pi} \int_0^{\infty} \text{Im} \left(-\frac{1}{\varepsilon(T')} \right) \frac{T' dT'}{T'^2 - T^2} \quad (8)$$

Hence, analysis of spectroscopic ellipsometry data with a suitable Tauc-Lorentz parameterization of the dielectric function of amorphous semiconductors [33] is useful to obtain the refractive index extrapolated to 0 eV, $n(0)$, which is needed in the inversion algorithm. Furthermore, the effective number of electrons per atom, N_{EFF} , involved in the dielectric function is determined applying the Bethe sum rule [25, 34]:

$$N_{\text{EFF}} = \frac{2\varepsilon_0 m_0}{\pi \hbar^2 N_{\text{AT}}} \int_0^{\infty} \text{Im} \left(-\frac{1}{\varepsilon(T)} \right) T dT \quad (9)$$

2.2 Contact angles and work of adhesion

Provided that roughness effects at the solid surface and chemical reactions at the solid carbon film / liquid (CL) interface are negligible, the contact angle θ at a rigid solid surface [35] contains information about the surface tensions of solid and liquid surfaces through Young's equation:

$$\gamma_{LV} \cos \theta = \gamma_{CV} - \gamma_{CL} \quad (10)$$

where γ_{LV} , γ_{CV} and γ_{CL} are respectively the interfacial tensions of the liquid-vapor, solid-vapor and solid-liquid interfaces. This equation reflects the equilibrium between cohesive forces in the liquid drop and adhesion forces at the liquid-solid interface [5]. In order to derive the solid surface tension, γ_{CV} , from the experimental values of γ_{LV} and θ , an estimate of the thermodynamic work of adhesion for a solid and a liquid in contact (Young-Dupré equation):

$$W_{CL} = (-\gamma_{CL} + \gamma_{CV} + \gamma_{LV}) = \gamma_{LV}(1 + \cos \theta) \quad (11)$$

has to be obtained.

One possibility (used in Method B, as detailed below) is to consider that W_{CL} can be taken as the geometric mean of the work of cohesion of the solid ($2\gamma_{CV}^d$) and the work of cohesion of the liquid ($2\gamma_{LV}^d$):

$$W_{CL} = 2 \left[\gamma_{CV}^d \gamma_{LV}^d \right]^{1/2} \quad (12)$$

hence the Rayleigh–Good equation is obtained for a purely dispersive liquid. Assuming additivity of dispersive (d) and polar (AB) components of the work of adhesion ($\gamma_{CV}^T = \gamma_{CV}^d + \gamma_{CV}^{AB}$), the acid-base model proposed by van Oss, Chaudury and Good [5, 36-38] introduces an asymmetric behavior in the polar component, γ^{AB} , including Lewis-acid (electron acceptor) and Lewis-base (electron donor) components, γ^+ and γ^- , leading to:

$$\gamma_{CL} = \gamma_{CV} + \gamma_{LV} - 2 \left[\left(\gamma_{CV}^d \gamma_{LV}^d \right)^{1/2} + \left(\gamma_{CV}^+ \gamma_{LV}^- \right)^{1/2} + \left(\gamma_{CV}^- \gamma_{LV}^+ \right)^{1/2} \right] \quad (13)$$

Since a non-polar liquid with only dispersive surface free energy interacts with only the dispersion component (γ_{CV}^d) of the solid, one non-polar liquid is used to derive the dispersive (or Lifshitz – van der Waals) component γ_{CV}^d from the contact angle equation:

$$(1 + \cos \theta) = 2 \left[\frac{\gamma_{CV}^d}{\gamma_{LV}^d} \right]^{1/2} \quad (14)$$

Within this multicomponent model of surface tension, at least two polar liquids are needed to obtain γ_{CV}^+ and γ_{CV}^- values. In order to describe the Lewis acid-base properties, carefully selected dispersive and polar liquids should be used in order to obtain intrinsic consistency and well-behaved data for fitting the polar work of adhesion. [21, 39]

In this work, DIM is used as nonpolar liquid because of its high surface tension ($\gamma_{LV}^d = 51.0$ mJ/m²) and water as a polar liquid ($\gamma_{LV}^d = 21.8$ mJ/m², $\gamma_{LV}^T = 72.8$ mJ/m²) due to its ubiquitous importance in applied physics and chemistry. Models for London dispersion spectra have been established for both dispersive and polar compounds [19-20] and we use these models for liquid water and diiodomethane, while for vacuum the dispersion spectrum is taken to be 1. Hence, γ_{CV}^d is determined for each carbon surface using θ_{DIM} (Table 2) and Eqn. 14. In the case of water (and any other polar liquid), for comparison with Hamaker energies, we are interested only in the dispersive part of the work of adhesion (Eqn. 12).

2.3 Hamaker energies and cutoff parameters

In the calculation of Hamaker energies, retardation and many-body effects are naturally incorporated in Lifshitz formalism (Eqn. 2-4), along with both transverse electric and transverse magnetic modes. Lifshitz model further assumes abrupt interfaces between homogeneous materials, i.e. at liquid surfaces, it excludes interface reorganization of surface active functionalities [40]. In the following, we consider two methods to retrieve cutoff distance and cutoff wave number at a liquid / solid interface, which requires the experimental contact angle, θ_{DIM} , and the tabulated surface tension of the liquid, γ_{LV}^d ; consistency between contact angle experiments and Lifshitz theory requires that $H_{0\ CVL}$ is not necessarily a constant.

Method A: The first approach follows previous analysis of dispersive liquids in contact with polymer surfaces [20, 41], where the energy of adhesion W_{CL} equals the van der Waals interaction free energy, $E_{CVL}(L)$, taken at the equilibrium distance $H_{0\ CVL}$; this method is based on the expressions for E_{123} (Eqn. 1) and W_{CL} (Eqn. 11), along with γ_{LV}^d and γ_{CV}^d (defined as half the work of cohesion of the liquid and the solid, respectively) given by:

$$\gamma_{LV}^d = \frac{A_{LVL}}{24\pi H_{0\ LVL}^2} \quad (15a)$$

$$\gamma_{CV}^d = \frac{A_{CVC}}{24\pi H_{0\ CVC}^2} \quad (15b)$$

The experimental contact angle of a dispersive liquid given by $(1 + \cos\theta)E_{LVL} = 2 E_{CVL}$ or:

$$1 + \cos\theta = \frac{2 A_{CVL}}{A_{LVL}} \left[\frac{H_{0\ LVL}}{H_{0\ CVL}} \right]^2 \quad (16)$$

along with calculated Hamaker energy values, A_{LVL} and A_{CVL} , provide the cutoff distance ratio ($H_{0\ LVL} / H_{0\ CVL}$). The tabulated surface tension value, γ_{LV}^d , for a purely dispersive liquid gives $H_{0\ LVL}$ (**Eqn. 15**) and $H_{0\ CVL}$ is thus obtained from **Eqn. 16**. Since this first method is restricted to non-polar liquids, a second method also valid for polar liquids is proposed.

Method B: The second approach is valid for all usual liquids with tabulated values of the dispersive component, γ_{LV}^d , of the surface tension. The limitation of method A is circumvented by using: (i) the geometric approximation for the work of adhesion given by **Eqn. 12**; (ii) the dispersive component, γ_{CV}^d , of the surface tension of the solid obtained from **Eqn. 14** for the contact angle of a dispersive liquid (e.g. DIM). Hence, the calculated Hamaker energy, A_{CVL} , value provides the cutoff distance $H_{0\ CVL}$ (and the cutoff wavenumber $k_{0\ CVL} \approx 1/H_{0\ CVL}$):

$$W_{CL} = 2 \left[\gamma_{CV}^d \gamma_{LV}^d \right]^{1/2} = \frac{A_{CVL}}{12\pi H_{0\ CVL}^2} \quad (17)$$

Once the cutoff distances have been obtained for the different configurations, the geometric mean and arithmetic mean values of $H_{0\ CVC}$ and $H_{0\ LVL}$ will be compared with $H_{0\ CVL}$ values, in order to check for the best combining rules [**16, 17, 20**]:

$$\text{geometric mean } H_{0\ CVL} = \left(H_{0\ LVL} H_{0\ CVC} \right)^{1/2} \quad (18a)$$

$$\text{arithmetic mean } H_{0\ CVL} = \left(H_{0\ LVL} + H_{0\ CVC} \right) / 2 \quad (18b)$$

Finally, the respective London dispersion functions and non-retarded Hamaker energies were calculated in different planar configurations with either vacuum, water or DIM as intervening medium (including C-Vacuum-C, C-Water-C, C-DIM-C, C-Vacuum-Water, C-Vacuum-DIM) which allows to search for some correlations between calculated A_{CVC} , A_{CLC} , A_{CVL} and A_{CLV} values, with expected validity over a wide range of disordered carbon-based materials.

3. Results

As expected from their variable $sp^3 / (sp^3 + sp^2)$ hybridization ratio, very different bulk ELF distributions (**Fig. 1.a**) have been derived from XPS-PEELS spectra (Supplementary Information, **Fig. S1**) for the four amorphous carbon films. As shown in detail in our previous work [25], the $\sigma+\pi$ plasmon peak energy increases in the series PL a-C:H (24 eV) < SP a-C:H (26.5 eV) < SP a-C (28 eV) < PLD a-C (31 eV) and reaches 34.5 eV in mc-diamond (**Table 1**).

Table 2 : Calculated Hamaker energies, A_{132} , cutoff wave numbers, $k_{0\ 132}$, and cutoff distances, $H_{0\ 132}$, of a-C and mc-diamond films derived using methods A and B (see text, **Section 2.3**). For the liquids, water and DIM, one obtains respectively: $A_{WVW} = 0.242$ eV, $A_{DVD} = 0.449$ eV, $k_{0\ WVW} = 6.51$ nm⁻¹, $k_{0\ DVD} = 7.30$ nm⁻¹, $H_{0\ WVW} = 0.154$ nm⁻¹, $H_{0\ DVD} = 0.137$ nm⁻¹.

Material	A_{CVC} (eV)	A_{CWC} (eV)	A_{CDC} (eV)	$k_{0\ CVC}$ (nm ⁻¹)	$k_{0\ CVD}$ [A, B] (nm ⁻¹)	$k_{0\ CVW}$ [B] (nm ⁻¹)	$H_{0\ CVC}$ (nm)	$H_{0\ CVD}$ [A, B] (nm)	$H_{0\ CVW}$ [B] (nm)
a-C Sputtered	1.164	0.460	0.260	4.21	5.66	5.32	0.237	0.177	0.188
a-C:H Plasma	1.232	0.496	0.309	3.71	5.36	5.01	0.270	0.187	0.200
a-C:H Sputtered	0.968	0.322	0.177	4.66	5.99	5.61	0.271	0.187	0.200
ta-C PLD	1.943	1.048	0.789	3.13	4.97	4.63	0.319	0.201	0.216
mc-diamond HF-CVD	1.924	1.024	0.778	3.28	5.11	4.74	0.305	0.196	0.211

The corresponding imaginary part of the dielectric function (**Fig. 1.b**) clearly shows distinct $\sigma-\sigma^*$ (15±1 eV) and $\pi-\pi^*$ (3.5 eV) contributions in the sp^2 -rich sputtered a-C film. In contrast, a narrow $\sigma-\sigma^*$ peak is observed at 9.5 eV in the plasma-deposited a-C:H film with small sp^2 C content. Finally, in the low-density sp^2 -rich sputtered a-C:H ($E_p = 26.5$ eV) and in the high-density PLD a-C ($E_p = 31$ eV) films, $\pi-\pi^*$ and $\sigma-\sigma^*$ transitions have nearly merged into a broad peak, extending from 5 eV to 15 eV at half maximum. A monotonous increase of the $\sigma-\sigma^*$ transition energy, from 9.5 eV to 15 eV, is observed as the sp^2 hybridization increases.

This set of very different disordered carbon-based materials is thus useful to examine some general trends in calculated Hamaker energies and in distance or wave number cutoff parameters.

3.1 Hamaker energies

The KK transform of the imaginary part of the dielectric function (**Eqn. 4**) provides the London dispersion spectrum which is a real function, monotonically decaying from $\epsilon_1(E=0)$ to 1, as frequency increases (**Fig. 2b**). Its strength is thus dependent on the normalization of PEELS data (**Eqn. 8**) performed using optical measurements in the near-infrared range (in this work, spectroscopic ellipsometry data near 1 eV).

Herein, for liquid water and diiodomethane, the London dispersion spectrum (**Fig. 2a**) was derived from index of refraction matching oscillator models given respectively by Shardt [19] and Drummond [20]. Comparison of Hamaker energies obtained using water and DIM as intervening medium are very interesting because they have very similar London dispersion in the EUV range, above 13 eV (**Fig. 2.a**) while they differ by a factor of about 1.5 in the UV-VIS-IR range. Hamaker energy $A_{LVL}(L)$ of parallel half spaces for a Liquid – Vacuum – Liquid configuration, at separation distance $L = 0.5$ nm, is 0.242 eV for water and 0.449 eV for DIM. Using γ_L^{LW} (DIM) = 51.0 mJ/m² and γ_L^{LW} (W) = 21.8 mJ/m², **Eqn. 15a** provides the respective cutoff distances $H_{0\ wvw} = 0.154$ nm and $H_{0\ dvd} = 0.137$ nm.

The role of intervening medium in the Hamaker energy $A_{131}(L)$ of parallel half spaces has been investigated in the Carbon – Vacuum – Carbon, Carbon – Water – Carbon and Carbon – DIM – Carbon configurations. The separation distance, $L = 0.5$ nm, used in the computation corresponds to the non-retarded dispersive interaction energy, since retardation effects become significant only beyond 2 nm (Supplementary Information, **Fig. S2**). **Fig. 3** shows partial Hamaker energies entering the spectral summations (**Eqn. 2**) giving $A_{CVC}(L)$, $A_{CWC}(L)$ and $A_{CDC}(L)$. The overall interaction strength decreases as the London dispersion function of the intervening medium gets stronger, arising from an important screening effect; e.g. at 10 eV, the partial Hamaker energy ratio values (A_{CDC}/A_{CVC}) are in the range 0.15–0.40 for this set of disordered carbons. In addition, the spectral weight strongly decreases in the IR-VIS range and shows a minor decrease in the UV-EUV range, resulting in stronger relative weight in the EUV range (10-120 eV) in particular with DIM as intervening liquid.

Integrated values of Hamaker energies are reported in **Table 2** for the CVC, CWC and CDC configurations for all disordered carbon films. Convergence of the sum is obtained for a high energy limit of the order of 100 eV. As expected from **Fig. 3**, a systematic decrease of the dispersive

interaction energy is observed as a function of increasing strength of the London dispersion function of the intervening medium ($A_{CVC} > A_{CWC} > A_{CDC}$).

Fig. 4 shows non-retarded ($L = 0.5$ nm) Hamaker dispersion energies calculated in different configurations: C-Vacuum-C, C-Water-C, C-DIM-C, C-Vacuum-Water, C-Vacuum-DIM; for both liquids, it gives evidence of a linear dependence between calculated values of A_{CVL} , A_{CLC} and A_{CLV} Hamaker energies, as a function of A_{CVC} . Interestingly, this correlation appears to be valid for a-C and mc-diamond, over a broad range of $sp^3 / (sp^2 + sp^3)$ average hybridization:

$$\text{DIM} \quad A_{CDC} = -0.53 + 0.682A_{CVC}, \quad A_{CVD} = +0.42 + 0.227A_{CVC}, \quad A_{CDV} = +0.05 - 0.273A_{CVC} \quad (19a)$$

$$\text{W} \quad A_{CWC} = -0.40 + 0.745A_{CVC}, \quad A_{C VW} = +0.30 + 0.182A_{CVC}, \quad A_{C WV} = -0.04 - 0.205A_{CVC} \quad (19b)$$

Comparison of the results obtained with water ($A_{WVW} = 0.242$ eV) and DIM ($A_{DVD} = 0.449$ eV), corresponding respectively to the open and filled symbols in **Figure 4**, indicates that A_{CLC} decreases (while A_{CVL} increases) as a function of increasing strength of the London dispersion function of the intervening liquid phase. Note that A_{CLV} values are always negative with a small difference found between liquid DIM and water (**Fig. 4**).

3.2 Cutoff distance and wavenumber parameters

The $H_{0\ CVC}$ values derived for the disordered carbons investigated in this work are in the range 0.23–0.32 nm (average value 0.28 ± 0.04 nm). Carbon-liquid equilibrium distances with both DIM and water are found in the range $H_{0\ CVL} = 0.19 \pm 0.02$ nm (**Table 2**); however, for each carbon surface, a larger distance is found for a contact with water, i.e. $(H_{0\ CVW} - H_{0\ CVD}) \approx 0.013$ nm is always positive.

In **Table 2**, for better comparison with the wave number range involved in PEELS ($q < q_C$ with $q_C \approx 15$ nm⁻¹), we have chosen to report the cutoff wavenumber, $k_{0\ CVL}$, taken as the inverse of cutoff separation distance, $H_{0\ CVL}$. This work shows that $k_{0\ CVL} \ll q_C$ for a wide variety of carbon films.

In the case of DIM, $k_{0\ CVL}$ values obtained from both methods A and B are fully consistent, as expected. Interestingly, with method B, the values of $k_{0\ CVL}$ are slightly smaller for water as

compared to DIM (less than 10% difference). The values of $k_{0\text{ }CVC}$, derived from **Eqn. 15**, range from 3.1 to 4.7 nm⁻¹, and they are systematically smaller than $k_{0\text{ }CVW}$ (4.6-5.6 nm⁻¹) with liquid water and $k_{0\text{ }CVD}$ (5.0-6.0 nm⁻¹) with liquid DIM, for all the investigated carbon surfaces.

Fig. 5 shows that the geometric average of $H_{0\text{ }CVC}$ and $H_{0\text{ }LVL}$ (using cutoff distances $H_{0\text{ }WWW} = 0.154$ nm and $H_{0\text{ }DVD} = 0.137$ nm) is a very good approximation of $H_{0\text{ }CVL}$, in contrast with the arithmetic average value (**Eqn. 18**).

4. Discussion

In this section, calculated Hamaker energy values are discussed in terms of their spectral weight, without considering retardation effects since all calculations were performed in the non-retarded regime, at separation distance $L = 0.5$ nm. The potential role of the q -dependence of the ELF and dielectric function $\varepsilon(q, \omega)$ is addressed and compared with previous works. Finally, the cutoff distances and cutoff wave numbers, derived from experimental contact angles and calculated Hamaker energy values, will be discussed for predictive purposes.

4.1 Hamaker interaction strength

In this XPS-PEELS study, kinetic energy losses of C1s photoelectrons have been obtained over a 50 eV range and the ELF was extrapolated beyond 100 eV; negligible differences in the dielectric function have been found for power-law extrapolation of the ELF as E^p , using different exponents ($p = 4$ to 6) [25]. Using a wide range of amorphous carbon and microcrystalline diamond films allows investigation of some tendencies in Hamaker interaction strength and cutoff parameters behavior. As far as the disordered carbon properties are concerned, some reasonable correlation between Hamaker energy A_{CVC} and real dielectric function $\varepsilon_1(E = 0)$ is found (**Fig. 6**), as expected from **Eqn. 4** and **Fig. 2b**. Similar trend has also been reported for a wide range of compounds [42]; however, some limitations of the XPS-PEELS method are discussed in **Section 4.4**.

For each disordered carbon surface, we observe that A_{CLC} decreases with increasing strength of London dispersion function of the intervening liquid phase. Comparison of DIM and water shows that large London dispersion value of the intervening liquid in the IR-visible range results in small values of partial Hamaker energies; extremely small Hamaker energy, A_{CLC} , is found for plasma-deposited a-C:H (0.31 eV), sputtered a-C (0.26 eV) and sputtered a-C:H (0.18 eV) with

DIM as intervening liquid (**Fig. 3c**). This result clearly illustrates the screening effect of the intervening medium on A_{CLC} values.

Rather than considering spectrally integrated values, this work focuses on detailed information derived from the spectral weight of partial Hamaker energies. **Fig. 3** shows that $A_{CLC}(E)$ is shifted towards higher energies as the London dispersion function of the intervening liquid gets stronger. With water, the maximum generally occurs in the near IR-visible range (**Fig. 3.b**), while with DIM, the shape of the spectral response depends strongly on the dielectric function of the carbon film (**Fig. 3.c**): the maximum is found in the near IR range for sp^2 -rich a-C, while for hydrogenated a-C:H films, sp^3 -rich ta-C and mc-diamond, it is located in the UV-EUV range ($E > 5$ eV). However, due to equidistant energies used in the spectral summation (**Eqn. 2**), the integrated Hamaker energy is strongly dominated by the dispersive interactions in the UV and EUV range (10-120 eV).

The above results may have a broad impact in self-assembly of nanoparticles or tribological applications. In the case of water, $A_{CWC} > A_{WWW}$ holds for all investigated carbon films because water has a small Hamaker energy, $A_{WWW} = 0.242$ eV (**Table 2**). In contrast, since DIM displays high Hamaker energy, $A_{DVD} = 0.449$ eV, we find three amorphous carbon samples (sputtered a-C:H, sputtered a-C and plasma a-C:H) with opposite behaviour, i.e. $A_{CDC} < A_{DVD}$ which means that the energetically favourable situation (at equilibrium) is an air-gap configuration between liquid coated solid surfaces (DVD) rather than a bridging DIM liquid configuration (CDC).

4.2 q -averaged dielectric function $\langle \varepsilon(q, \omega) \rangle_q$

It is emphasized that calculation of Hamaker energy based on a q -averaged $\langle \varepsilon(q, \omega) \rangle_q$ dielectric function, as obtained from XPS-PEELS analysis of the solid surface, slightly modifies Δ_{jk}^* and Δ_{jk} values (**Eqn. 3**) obtained for disordered carbons and usual liquids. Since the plasmon energy $E_p(q)$ of the solid is displaced to higher energy values as compared with the plasma oscillation in the optical limit, $E_p(q=0)$, partial Hamaker components are decreased at energies near $E_p(q=0)$ and increased at higher energies. The overall Hamaker energy is weakly affected but some stronger retardation effects are expected.

To estimate the effect of the transferred wave vector in $\varepsilon(q, \omega)$ on calculated A_{132} values, a semi-quantitative evaluation should take into account: (i) the $(1/q)$ weighting factor (**Eqn. 6**) given by the physics of bulk plasmon excitation, (ii) the cutoff wave vector, q_C , due to plasmon decay

into single-particle excitations, e.g. for amorphous carbon, $q_C \approx 15 \text{ nm}^{-1}$ has been estimated in a free electron gas approximation [25], and (iii) the plasmon energy $E_p(q)$ dependence. The latter characteristic has been derived from scattering angle-resolved EELS experiments [43] for amorphous carbon with a relatively low atom density ($E_p = 22.8 \text{ eV}$):

$$E_p(q) = E_p(q=0) + D_q a_0^2 k_0^2 \theta^2 = E_p(q=0) + D_q (a_0 q)^2 \quad (20)$$

with a dispersion coefficient $D_q = 10.85 \text{ eV}$. This value coincides with the free electron approximation $\alpha = \frac{3 E_F}{5 E_p} = \frac{D_q / 2}{13.6}$ if $E_F = 15.2 \text{ eV}$. Simulations show that this $E_p(q)$ behaviour introduces additional contributions to the measured ELF in the energy range $E_p - 2E_p$, as compared with the optical limit. With an upper limit $q_C \approx 15 \text{ nm}^{-1}$ and the typical D_q value estimated for a-C, one obtains some weak contributions to the ELF displaced to higher energies, by an amount up to $E_L(q_C) - E_p(q=0) = D_q (a_0 q)^2 \approx 6 \text{ eV}$ (at the expense of ELF components near $E_p(q=0)$).

Prediction of losses in microcrystalline diamond is much more complex due to anisotropy of plasmon excitation and $E_p(q)$ dispersion [44] and to the textured crystalline orientation typically observed in mc-diamond thin films [24]. However, comparison between spectral weights of Hamaker energies obtained from our q -averaged $\langle \varepsilon(q, \omega) \rangle_q$ and that derived from optical data $\varepsilon(q=0, \omega)$ [45] indicates that the decreased interaction below $E_p(q=0) \approx 34 \text{ eV}$ is nearly compensated by the increased interaction above $E_p(q=0)$ (Supplementary Information, **Fig. S3**).

In the context of van der Waals energy computations, previous derivation of the dielectric function over a very broad energy range has been performed either by vacuum ultraviolet spectroscopy ($q = 0$, optical limit) [46] or by EELS at low loss energy, also called VEELS for Valence Electron Energy Loss Spectroscopy [47]. Note that in VEELS, the q -range for ELF integration depends on the angular deflection and the analyzer resolution, e.g. with 100 keV primary electron beam, a spectrometer collection angle of 9 mrad corresponds to an integration over scattering vectors out to $q = 2.4 \text{ nm}^{-1}$ [48, 49]. Since previous high resolution EELS experiments were typically performed using $q_{VEELS} = 1.0 \text{ nm}^{-1}$ (a-C:H) [50], $q_{VEELS} = 1.5 \text{ nm}^{-1}$ (ta-C) [51] or $q_{VEELS} = 2.0 \text{ nm}^{-1}$ (oxides) [49], the dispersive behavior of plasmon excitation is probably not fully captured in VEELS experiments ($q_{VEELS} \ll q_C$).

4.3 Cutoff distance and cutoff wave number

Some comparison with previous investigations of liquids can be useful to check for consistency of the method. In this study, the cutoff wavenumber $k_{0\ wvw} = 6.51\ \text{nm}^{-1}$ (0.154 nm) for water is larger than that obtained in previous simplified calculations of $k_{0\ wvw} = 4.76\ \text{nm}^{-1}$ (0.210 nm) derived using the same Parsegian representation [19]. In addition, the equilibrium distances, $H_{0\ wvw} = 0.154\ \text{nm}$ and $H_{0\ dvd} = 0.137\ \text{nm}$ for water and DIM respectively, obtained from the calculated Hamaker energy and tabulated liquid surface tension, are slightly smaller than the standard reference value, $H_0 = 0.16\ \text{nm}$ for liquid pairs [40].

For disordered carbon surfaces, the Hamaker cutoff wave numbers $k_{0\ cvc}$ obtained in this work, taken as the inverse of cutoff separation distance $H_{0\ cvc}$, have been found in the range from 3.1 to 4.7 nm^{-1} . They are consistent with the value $k_{0\ cvc} = 3.60\ \text{nm}^{-1}$ obtained with similar theoretical approach in a previous investigation of a-C films used as magnetic disk coatings [12].

For the selected amorphous carbon surfaces reported in **Table 2**, since $H_{0\ cvc} > H_{0\ lvl}$ one also finds $H_{0\ cvl} > H_{0\ lvl}$ for both liquids, with nearly constant ratio, $H_{0\ cvl} = (1.4 \pm 0.2) H_{0\ lvl}$. Similarly, a nearly constant ratio $H_{0\ cvw} \approx 1.07 H_{0\ cvd}$ is observed. The cutoff wave number globally decreases i.e. the cutoff distance increases, with increasing sp^3 hybridization (**Fig. 6b**); this result confirms the conventional view that the equilibrium distance should reflect an average interatomic distance. Overall, this work indicates that the cutoff distance value is not unique for different allotropes of the same condensed phase material.

4.4 Predictive relationships

The linear correlation between Hamaker energy A_{cvc} at room-temperature and real dielectric function in the IR range, $\varepsilon_1(E=0)$, shown in **Fig. 6**, can be used for predictive purposes:

$$A_{cvc} = [\varepsilon_1(E=0) - 1] \times 0.38\ \text{eV} \quad (21)$$

However, the sp^2 -rich hydrogen-free (sputtered) a-C film appears to depart from the regression line in **Fig. 6**, and deserves additional comment. As discussed in our previous work [25], the accuracy and reproducibility of PEELS data treatment depends primarily on the quality of zero-loss peak removal; for ta-C and a-C:H films with a large bandgap energy value (weak π - π^* transitions), robust results have been obtained and several methods provide essentially similar ELF and

dielectric function [25]. However, energy losses smaller than about 1 eV remain beyond the capability of the current XPS-PEELS method and further improvements are crucial for the investigation of some sp²-rich a-C and other materials which display a strong Drude contribution at very low energy [52].

Some limitations of this modelling of Hamaker energy should also be addressed. Possible interface reorganization of surface active functionalities in the liquid phase [40], e.g. preferential dipole orientation of water or DIM molecules at the interface are not considered in Lifshitz theory.

Finally, a linear dependence has been found between calculated A_{CVL} , A_{CLC} , A_{CLV} and A_{CVC} values, using water and DIM (Eqn. 19). It would be interesting to check whether other usual liquids also follow similar linear trend. Assuming that this behavior can be extrapolated to other disordered carbons, then the calculated A_{CVC} value can be used to predict Hamaker energies in other configurations (for a given liquid).

On the other hand, Eqn. 15b implies that an approximated value of A_{CVC} for any disordered carbon material with unknown dielectric function, can be derived from the dispersive component of the surface tension, γ_{CV}^d , and a guess value of the cutoff distance, $H_{0\ CVC}$, of the solid. In practice, the dispersive component of the surface tension, γ_{CV}^d , is readily obtained from the experimental contact angle with DIM (Eqn. 14) while an average value of $H_{0\ CVC} = 0.28 \pm 0.04$ nm (Table 2), for disordered carbons can be tentatively used in first approximation.

5. Conclusion

This work shows that q -averaged $\langle \varepsilon(q, \omega) \rangle_q$ dielectric functions derived from experimental energy losses of photoelectrons (XPS-PEELS) can be used to calculate non-retarded and retarded Hamaker energies in CVL, CVC and LVL configurations (L = DIM or Water). In contrast with previous VEELS experiments, this q -averaged $\langle \varepsilon(q, \omega) \rangle_q$ captures the whole range of wave numbers up to the cutoff q_C given by the physics of plasmon excitation (14 ± 1 nm⁻¹ in disordered carbons). The q -dependence of plasmon energy, $E_p(q)$, slightly increases London contributions to Hamaker energy above $E_p(q = 0)$, as illustrated in this study by mc-diamond.

Typical cutoff wavenumbers for Hamaker interaction, $k_{0\ CVC}$, are found in the range 3.1 – 4.7 nm⁻¹, hence $k_{0\ CVC} \ll q_C$ for a wide variety of carbon films. It appears that the cutoff wave number for solid-liquid contacts cannot be considered as a constant and extends previous

conclusions drawn for liquid pairs [19]. For amorphous carbon and microcrystalline diamond films, the geometric average approximation holds for the solid-liquid equilibrium distance ($H_{0\ CVL}$) $H_{0\ CVL}^2 = H_{0\ LVL} H_{0\ CVC}$ and some linear dependence is found for A_{CVL} , A_{CLC} , A_{CLV} as a function of A_{CVC} values, for both DIM and water. More generally, once correlations between calculated Hamaker energies have been established for a given liquid (see e.g. **Eqn. 19**), predictive relationships for solids with unknown dielectric function only require some independent experimental determination of γ_{CV}^d and a guess value for $H_{0\ CVC}$ of the solid.

Acknowledgments

One of us (C.G.) is grateful to CNPq agency for a visiting researcher grant (PVE 400691/2012-4) in the *Ciência Sem Fronteiras* programme. One of us (D.D.) is grateful to CAPES agency (Brazil) for a senior researcher grant (CAPES BEX 0281/15-8). The authors acknowledge K. Zellama (LPMC, Amiens University) for sputtered a-C films, J.P. Conde and V. Chu (INESC-MN, Lisbon) for plasma deposition of a-C:H films, S. Députier, A. Perrin and M. Guilloux-Viry (LCSIM, Rennes University) for pulsed laser deposition of a-C films, and D. Ballutaud for mc-diamond films.

REFERENCES

- [1] E.M. Lifshitz, The Theory of Molecular Attractive Forces between Solids, Sov. Phys. JETP **2**, 73 (1956)
- [2] I.E. Dyaloshinski, E.M. Lifshitz, L.P. Pitaevski, General Theory of van der Waals' forces, Adv. Phys. **10**, 165 (1961)
- [3] J. Mahanty, B.W. Ninham, *Dispersion forces* (Academic Press, London, 1976)
- [4] J.N. Israelachvili, *Intermolecular and Surface Forces* (Academic Press, London, 1992)
- [5] C.J. van Oss, *Interfacial forces in aqueous media* (Marcel Dekker, New York, 1994)
- [6] R.R. Dagastine, D.C. Prieve, L.R. White, Calculations of van der Waals forces in 2-Dimensionally Anisotropic Materials and Its Application to Carbon Black, J. Colloid Interface Sci. **249**, 78 (2002) DOI: 10.1006/jcis.2002.8239
- [7] R.F. Rajter, R.H. French, W.Y. Ching, W.C. Carter, Y.M. Chiang, Calculating van der Waals-London dispersion spectra and Hamaker coefficients of carbon nanotubes in water from *ab initio* optical properties, J. Appl. Phys. **101**, 054303 (2007) DOI: 10.1063/1.2709576
- [8] R.B. dos Santos, F. de Brito Mota, R. Rivelino, A theoretical evaluation of the effect of water on the electronic properties of low density amorphous carbon nanoparticles, Carbon **50**, 2788 (2012) DOI: 10.1016/j.carbon.2012.02.041
- [9] M. Rahmat, P. Hubert, Carbon nanotube-polymer interactions in nanocomposites: a review, Compos. Sci. Technol. **72**, 72 (2011) DOI: 10.1016/j.compscitech.2011.10.002
- [10] R.R. Dagastine, L.R. White, P.M. Jones, Y.T. Hsia, Effect of media overcoat on van der Waals interaction at the head-disk interface, J. Appl. Phys. **97**, 126106 (2005) DOI: 10.1063/1.1941464
- [11] B. Marchon, T.E. Karis, Poiseuille flow at a nanometer scale, Europhys. Lett. **74**, 294 (2006) DOI: 10.1209/epl/i2005-10520-5
- [12] T.E. Karis, X.C. Guo, J.Y. Juang, Dynamics in the Bridged State of a Magnetic Recording Slider, Tribol. Lett. **30**, 123 (2008) DOI: 10.1007/s11249-008-9319-0
- [13] C. Noguez, C.E. Roman-Velazquez, Dispersive force between dissimilar materials: Geometrical effects, Phys. Rev. B **70**, 195412 (2004) DOI : 10.1103/PhysRevB.70.195412
- [14] V.V. Nesterenko, I.G. Pirozhenko, Lifshitz formula by a spectral summation method, Phys. Rev. A **86**, 052503 (2012) DOI: 10.1103/PhysRevA.86.052503
- [15] J.L. Li, J. Chun, N.S. Wingreen, R. Car, I.A. Aksay, D.A. Saville, Use of dielectric functions in the theory of dispersion forces, Phys. Rev. B **71**, 235412 (2005) DOI: 10.1103/PhysRevB.71.235412
- [16] D.C. Prieve, W.B. Russel, Simplified predictions of Hamaker constants from Lifshitz theory, J. Colloid Interface Sci. **125**, 1 (1988) DOI: 10.1016/0021-9797(88)90048-3
- [17] D.B. Hough, L.R. White, The calculation of Hamaker constants from Lifshitz theory with applications to wetting phenomena, Adv. Colloid Interface Sci. **14**, 3 (1980) DOI: 10.1016/0001-8686(80)80006-6
- [18] L.R. White, van der Waals interaction energy and disjoining pressure at small separation, J. Colloid Interface Sci. **343**, 338 (2010) DOI: 10.1016/j.jcis.2009.11.002
- [19] N. Shardt, S. Bhattacharjee, J.A.W. Elliott, Evaluation of the Constant Wavenumber Cutoff Parameter for Modeling van der Waals Energy, J. Phys. Chem. C **118**, 3539 (2014) DOI: 10.1021/jp410199j
- [20] C.J. Drummond, D.Y.C. Chan, van der Waals Interaction, Surface Free Energies, and Contact Angles: Dispersive Polymers and Liquids, Langmuir **13**, 3890 (1997) DOI: 10.1021/la962131c

- [21] A. Zebda, H. Sabbah, S. Ababou-Girard, F. Solal, C. Godet, Surface energy and hybridization studies of amorphous carbon surfaces, *Appl. Surf. Sci.* **254**, 4980 (2008) DOI: 10.1016/j.apsusc.2008.01.147
- [22] C. Godet, D. David, H. Sabbah, S. Ababou-Girard, F. Solal, Bulk and surface plasmon excitations in amorphous carbon films measured by core-level loss spectroscopy, *Appl. Surf. Sci.* **255**, 6598 (2009) DOI: 10.1016/j.apsusc.2009.02.050
- [23] H. Sabbah, S. Ababou-Girard, A. Zebda, D. David, B. Fabre, S. Députier, A. Perrin, M. Guilloux-Viry, F. Solal, C. Godet, Thermal grafting of organic monolayers on amorphous carbon and silicon (111) surfaces: A comparative study, *Diam. Relat. Mater.* **18**, 1074 (2009) DOI: 10.1016/j.diamond.2009.01.037
- [24] D. David, M.A. Pinault-Thaury, D. Ballutaud, C. Godet, Sensitivity of photoelectron energy loss spectroscopy to surface reconstruction of microcrystalline diamond films, *Appl. Surf. Sci.* **273**, 607 (2013) DOI : 10.1016/j.apsusc.2013.02.087
- [25] D. David, C. Godet, Derivation of dielectric function and inelastic mean free path from photoelectron energy-loss spectra of amorphous carbon surfaces, *Appl. Surf. Sci.* **387**, 1125 (2016) DOI: 10.1016/j.apsusc.2016.06.044
- [26] J. Robertson, Diamond-like amorphous carbon, *Mat. Sci. Eng. R* **37**, 129 (2002) DOI: 10.1016/S0927-796X(02)00005-0
- [27] C. Godet, T. Heitz, J.E. Bourée, B. Drévilion, C. Clerc, Growth and composition of dual-plasma polymer-like amorphous carbon films, *J. Appl. Phys.* **84**, 3919 (1998) DOI : 10.1063/1.368570
- [28] S. Ababou-Girard, F. Solal, B. Fabre, F. Alibert, C. Godet, Covalent grafting of organic molecular chains on amorphous carbon surfaces, *J. Non-Cryst. Solids* **352**, 2011 (2006) DOI : 10.1016/j.jnoncrysol.2005.10.040
- [29] S. Hufner, *Photoelectron Spectroscopy* (Springer series in Solid-State Sciences vol. 82, Springer, Berlin, 1995)
- [30] A.C. Simonsen, F. Yubero, S. Tougaard, Quantitative model of electron energy loss in XPS, *Phys. Rev. B* **56**, 1612 (1997) DOI: 10.1103/PhysRevB.56.1612
- [31] W.S.M. Werner, P. Schattschneider, On the energy dissipation process in incoherent electron scattering, *J. Electron Spectrosc. Relat. Phen.* **143**, 65 (2005) DOI: 10.1016/j.elspec.2004.03.011
- [32] P. Nozières, D. Pines, Electron Interaction in Solids. Characteristic Energy Loss Spectrum, *Phys. Rev.* **113**, 1254 (1959) DOI: 10.1103/PhysRev.113.1254
- [33] T. Katsuno, C. Godet, J.C. Orlianges, A.-S. Loir, F. Garrelie, A. Catherinot, Optical properties of high-density amorphous carbon films grown by nanosecond and femtosecond pulsed laser ablation, *Appl. Phys. A* **81**, 471 (2005) DOI: 10.1007/s00339-005-3257-6
- [34] D.Y. Smith, E. Shiles, Finite-energy f -sum rules for valence electrons, *Phys. Rev. B* **17**, 4689 (1978) DOI: 10.1103/PhysRevB.17.4689
- [35] R.W. Style, R. Boltyanskiy, Y. Che, J.S. Wettlaufer, L.A. Wilen, E.R. Dufresne, Universal Deformation of Soft Substrates Near a Contact Line and the Direct Measurement of Solid Surface Stresses, *Phys. Rev. Lett.* **110**, 066103 (2013) DOI: 10.1103/PhysRevLett.110.066103
- [36] C.J. van Oss, M.K. Chaudhury, R.J. Good, Interfacial Lifshitz-van der Waals and polar interactions in macroscopic systems, *Chem. Rev.* **88**, 927 (1988) DOI: 10.1021/cr00088a006
- [37] P.A. Kollman, Noncovalent interactions, *Acc. Chem. Res.* **10**, 365 (1977) DOI: 10.1021/ar50118a003
- [38] N.T. Correia, J.J. Moura Ramos, B.J.V. Saramago, J.C.G. Calado, Estimation of the Surface Tension of a Solid: Application to a Liquid Crystalline Polymer, *J. Colloid. Interface Sci.* **189**, 361 (1997) DOI: 10.1006/jcis.1997.4857

- [39] C. Della Volpe, D. Maniglio, M. Brugnara, S. Siboni, M. Morra, The solid surface free energy calculation: I. In defense of the multicomponent approach, *J. Colloid Interface Sci.* **271**, 434 (2004) DOI: 10.1016/j.jcis.2003.09.049
- [40] S. Chevalier, M.K. Chaudhury, Further reflections on the geometric mean combining rule for interfacial tension, *Langmuir* **31**, 11296 (2015) DOI: 10.1021/acs.langmuir.5b03054
- [41] A. El Ghzaoui, Determination of contact angles: Consistency between experiment and theory, *J. Appl. Phys.* **86**, 2920 (1999) DOI: 10.1063/1.371143
- [42] R.H. French, R.M. Cannon, L.K. DeNoyer, Y.M. Chiang, Full spectral calculation of non-retarded Hamaker constants for ceramic systems from interband transition strengths, *Solid State Ionics* **75**, 13 (1995) DOI: 10.1016/0167-2738(94)00217-G
- [43] H. Roth, K. Lang, M. Ebelshäuser, D. Lang, H. Schmoranzer, Electron energy-loss spectrometry of thin amorphous carbon films: Accurate determination of the plasmon energy, *Phys. Lett. A* **235**, 551 (1997) DOI: 10.1016/S0375-9601(97)00658-0
- [44] S. Waidmann, M. Knupfer, B. Arnold, J. Fink, A. Fleszar, W. Hanke, Local-field effects and anisotropic plasmon dispersion in diamond, *Phys. Rev. B* **61**, 10149 (2000) DOI: 10.1103/PhysRevB.61.10149
- [45] D.F. Edwards, H.R. Philipps, E.D. Palik (Ed.), *Handbook of Optical Constants of Solids* (Academic, San Diego, 1985), p. 665
- [46] R.H. French, H. Müllejans, D.J. Jones, Optical Properties of Aluminum Oxide: Determined from Vacuum Ultraviolet and Electron Energy-Loss Spectroscopies, *J. Am. Ceram. Soc.* **81**, 2549 (1998) DOI: 10.1111/j.1151-2916.1998.tb02660.x
- [47] R.H. French, Origins and Applications of London Dispersion Forces and Hamaker Constants in Ceramics, *J. Am. Ceram. Soc.* **83**, 2117 (2000) DOI: 10.1111/j.1151-2916.2000.tb01527
- [48] J. Kulik, Y. Lifshitz, G.D. Lempert, J.W. Rabalais, D. Marton, Electron energy-loss spectroscopy of mass-selected ion-beam-deposited diamondlike carbon, *J. Appl. Phys.* **76**, 5063 (1994) DOI: 10.1063/1.357218
- [49] H. Müllejans, R.H. French, Interband electronic structure of a near- $\Sigma 11$ grain boundary in α -alumina determined by spatially resolved valence electron energy-loss spectroscopy, *J. Phys. D : Appl. Phys.* **29**, 1751 (1996) DOI: 10.1088/0022-3727/29/7/010
- [50] J. Fink, Th. Müller-Heinzerling, J. Pflüger, B. Scheerer, B. Dischler, P. Koidl, A. Bubenzer, R.E. Sah, Investigation of hydrocarbon-plasma-generated carbon films by electron-energy-loss spectroscopy, *Phys. Rev. B* **30**, 4713 (1984) DOI: 10.1103/PhysRevB.30.4713
- [51] S. Waidmann, M. Knupfer, J. Fink, B. Kleinsorge, J. Robertson, Electronic structure studies of undoped and nitrogen-doped tetrahedral amorphous carbon using high-resolution electron energy-loss spectroscopy, *J. Appl. Phys.* **89**, 3783 (2001) DOI: 10.1063/1.1350999.
- [52] T.T.P. Cheung, X-ray photoemission of polynuclear aromatic carbon, *J. Appl. Phys.* **55**, 1388 (1984) DOI: 10.1063/1.333229

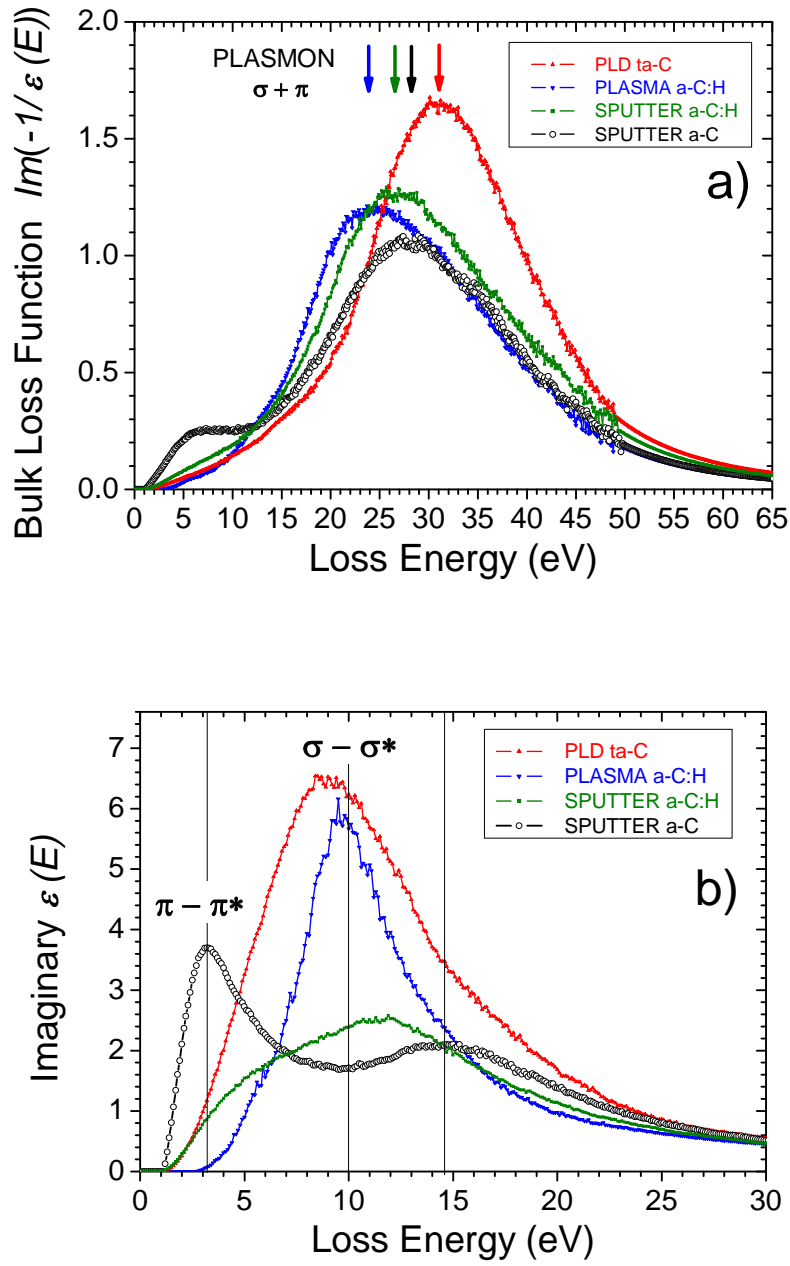


Fig. 1. PEELS analysis (normal emission angle, $\alpha = 0^\circ$) of amorphous carbon surfaces, PLD ta-C, plasma a-C:H, sputtered a-C:H and sputtered a-C : a) bulk energy loss function with high energy extrapolation as E^{-6} . b) Imaginary part of the dielectric function $\epsilon(E)$.

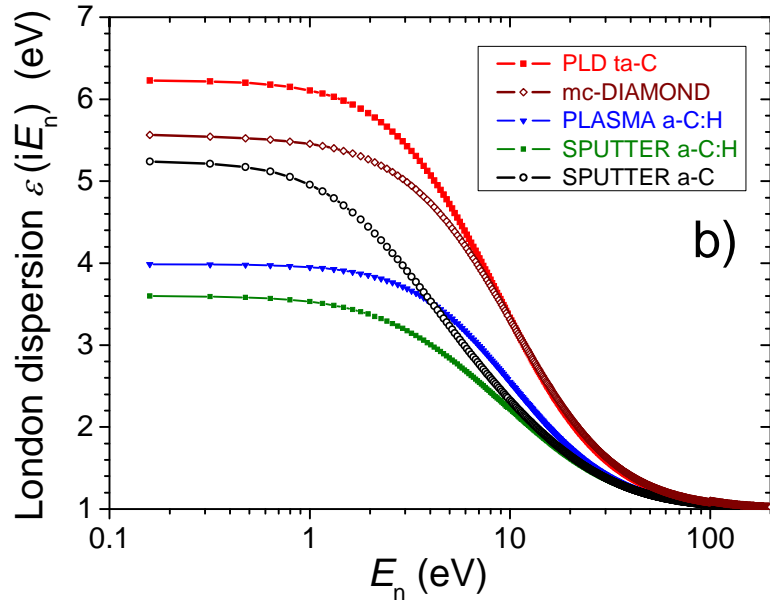
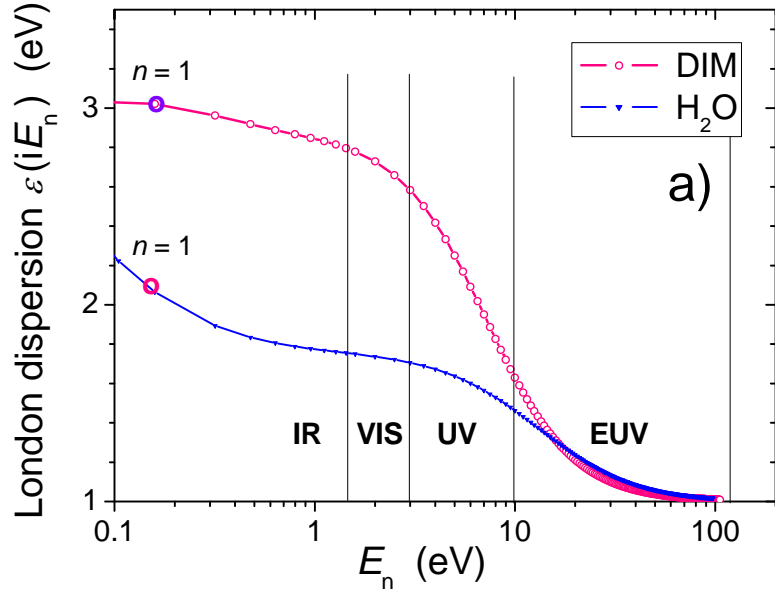


Fig. 2. London dispersion spectra: a) diiodomethane (DIM) and water (H_2O), b) PLD ta-C, mc-diamond, plasma a-C:H, sputtered a-C:H and sputtered a-C. Data at $\hbar\zeta_n = 0 \text{ eV}$ ($n = 0$) are not shown for DIM (5.32) and water (78.8). The bold circles in (a) and the first point in (b) are located at $\hbar\zeta_n = n 2\pi k_B T = 0.157 \text{ eV}$ ($n = 1$).

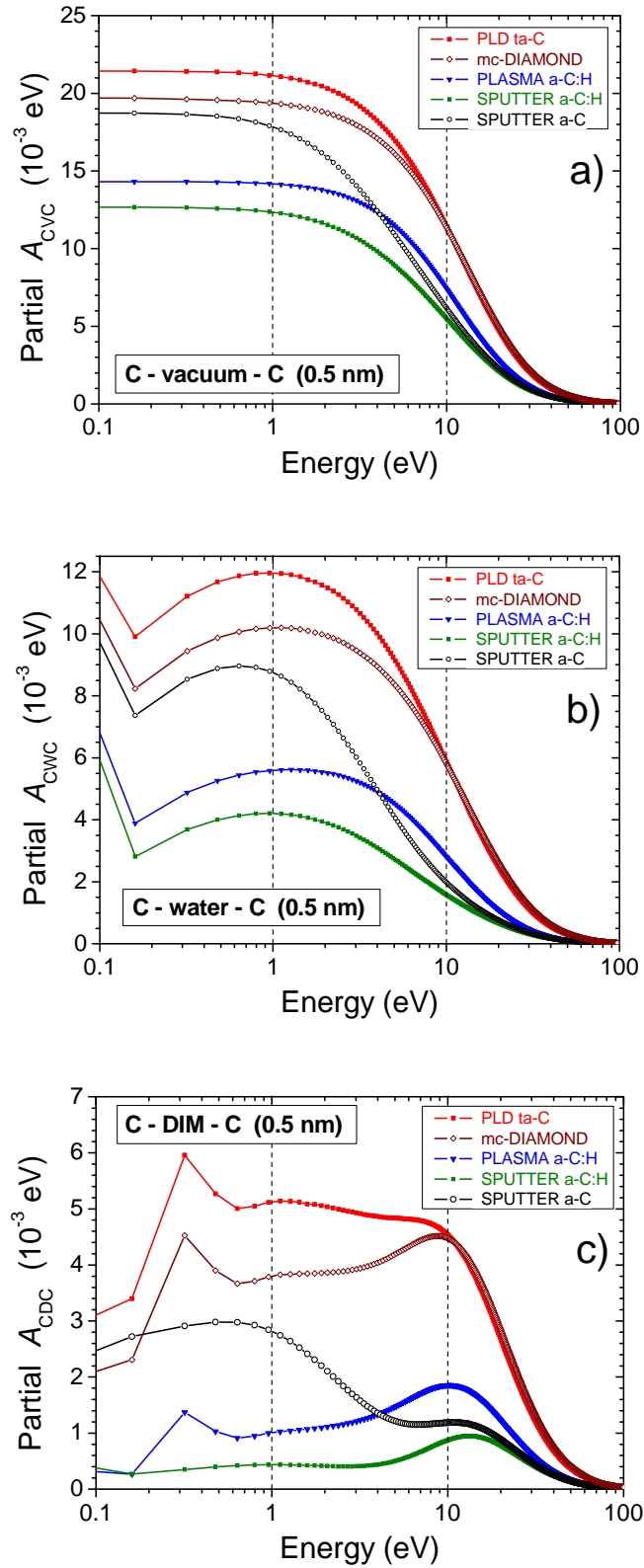


Fig. 3. Partial non-retarded Hamaker energies at $L = 0.5$ nm, for C-Vacuum-C (a), C-Water-C (b), C-DIM-C (c) configurations. Note that the spectral weight is shifted to the UV range and the overall strength is decreased as the London dispersion function of the intervening medium gets stronger.

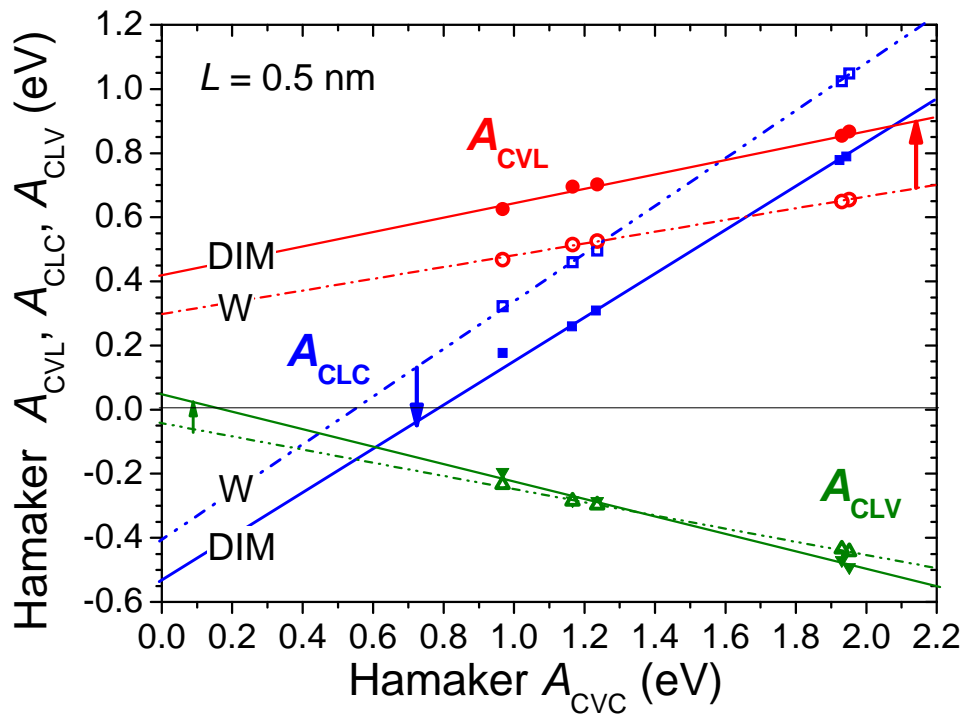


Fig. 4. Calculated A_{CVL} (circles), A_{CLC} (squares) and A_{CLV} (triangles) Hamaker energies for a-C and mc-diamond surfaces, showing a linear correlation with A_{CVC} given by **Eqn. 19** (water: open symbols and dash-dotted lines, DIM: full symbols and bold lines). The arrows represent the tendency with increasing strength of the London dispersion function of the liquid medium.

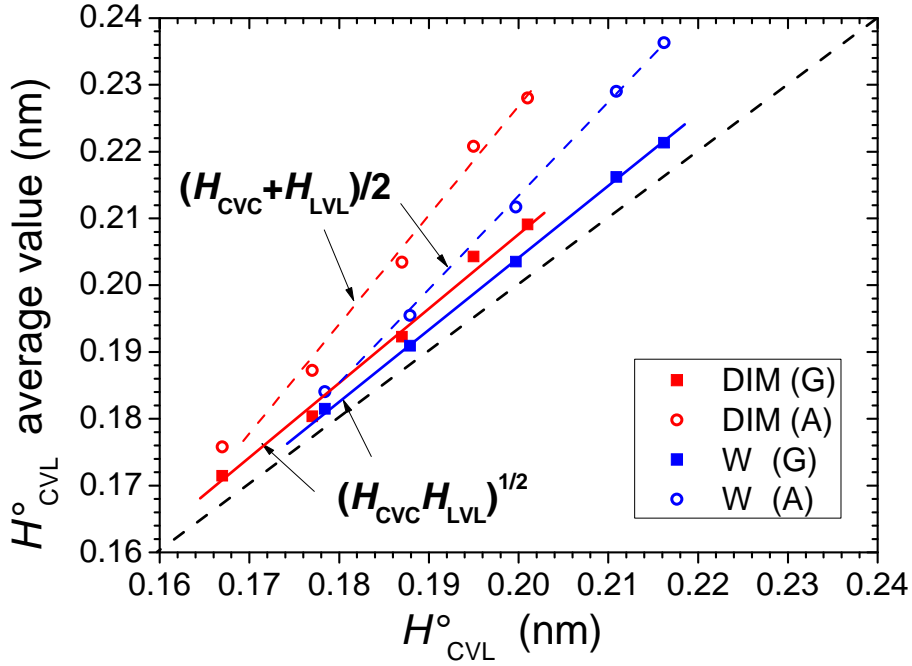


Fig. 5. Approximations of $H_{0\text{ CVL}}$, using geometric (G) and arithmetic (A) averages of $H_{0\text{ CVC}}$ and $H_{0\text{ LVL}}$ (**Eqn 18**). The lines are guides-to-the-eye.

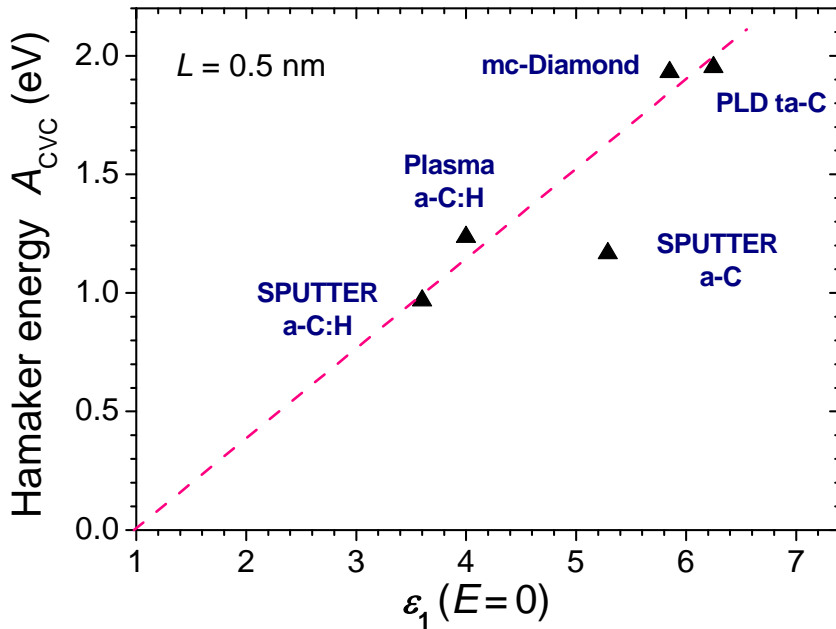


Fig. 6. Calculated A_{CVC} Hamaker energy for a-C and mc-diamond films, showing a linear correlation with the real dielectric function in the IR range (**Eqn. 21**).

SUPPLEMENTARY INFORMATION

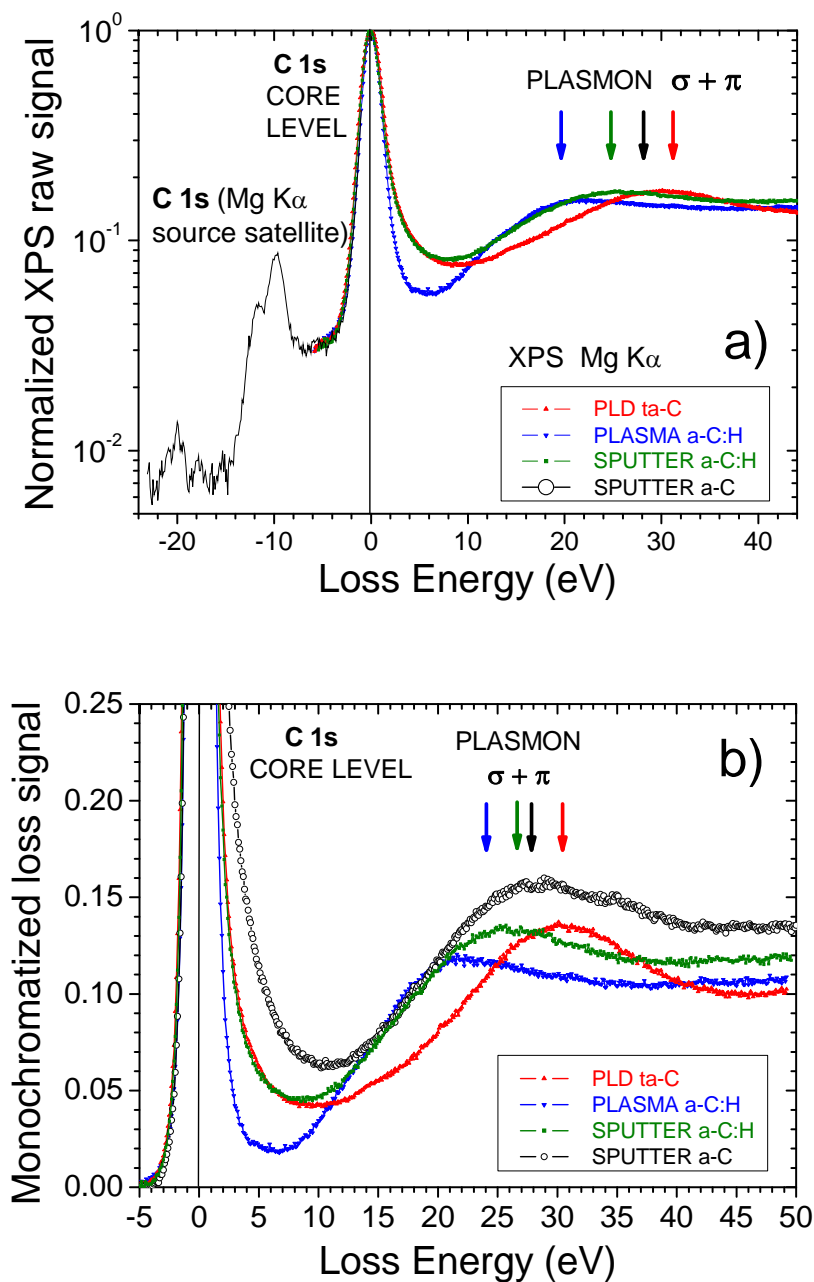


Fig. S1 XPS-PEELS spectra measured at normal emission angle ($\alpha = 0^\circ$), for different a-C films with variable sp^2 - sp^3 content and $(\sigma+\pi)$ plasmon energy: a) Raw XPS spectra obtained with non-monochromatic Mg $K\alpha$ X-ray source (1253.6 eV) ; b) numerically monochromatized loss spectra $J(T)$ using satellites $K\alpha_3/K\alpha_{1,2} = 0.08$ and $K\alpha_4/K\alpha_{1,2} = 0.04$ at -8.4 and -10.2 eV, respectively.

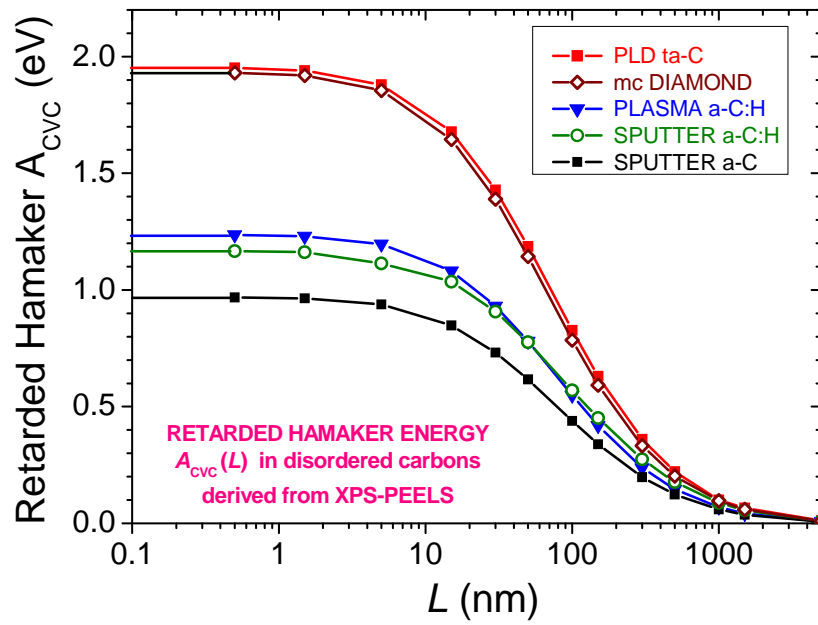


Fig. S2 Retarded Hamaker interaction energy $A_{CVC}(L)$ for disordered carbon films.

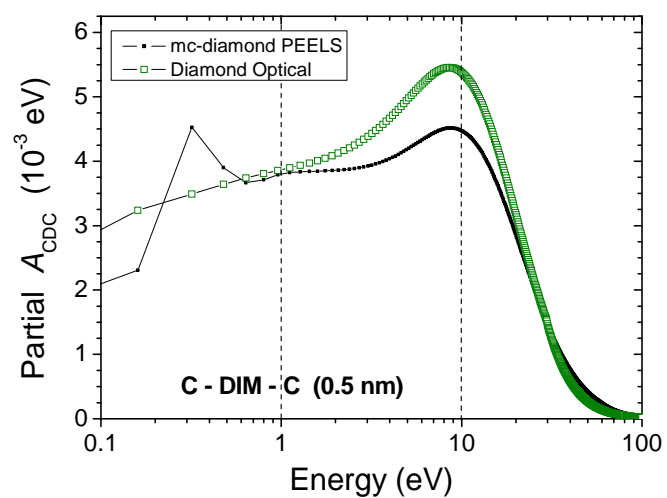
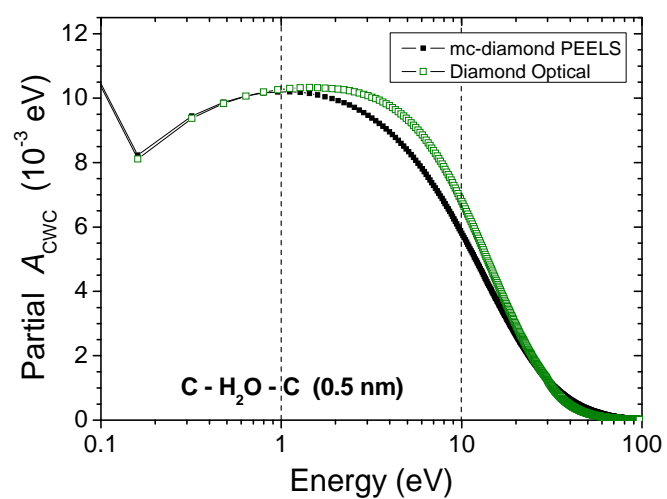
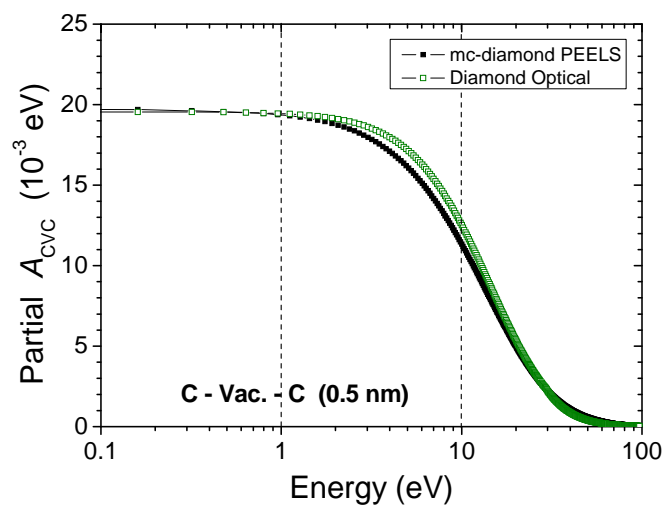


Fig. S3 Partial Hamaker interaction A_{CLC} ($L = \text{vacuum, water, DIM}$), using experimental XPS-PEELS data for mc-diamond or tabulated optical dielectric function of diamond (**Ref. 45**).